

Case study: measurement of Q and cumulative attenuation from VSP data

Gary F. Margrave, Devon Canada Corporation

SUMMARY

The measurement of attenuation in seismic data is described and analyzed. The measurement problem is defined as the estimation of the attenuation parameter Q or the estimation of the related quantity CA (cumulative attenuation) or both. Two very different estimation techniques are described: the spectral-ratio method (SRM), which is well-known, and the dominant-frequency method, which is mostly new here. The strengths and weaknesses of both methods are discussed and the extension to CA is given. It is demonstrated that CA estimates are more stable than Q estimates when attenuation is weak. The application of these techniques is demonstrated on a zero-offset VSP with a vibroseis source. Using the shallowest receiver (2185ft) as a reference, attenuation estimates were obtained for all receivers at depths equal to or greater than 5000ft. Consistent estimates were obtained from both the SRM and the DFM but it is demonstrated that any residual upcoming waves in the downgoing wave cause considerable error. The possibility of extending these measurements to the earth's surface by assuming the reference wave there is the Klauder wavelet is examined. The results are plausible and seem appropriate to apply to surface recordings for bandwidth enhancement.

INTRODUCTION

Anelastic attenuation is arguably the single most important factor limiting the resolution of seismic images. Since the earth is not a perfect elastic medium, seismic waves undergo progressive energy loss as they propagate. This loss is usually thought of as a conversion of wave energy to heat as the seismic motion causes internal friction in the rock. Calling this effect “intrinsic attenuation”, there is also a second effect, called “stratigraphic attenuation” that has nothing to do with anelasticity and everything to do with fine layering. Stratigraphic attenuation, first predicted and described by O’Doherty and Anstey (1971), is not an actual energy loss but is an interference effect resulting from the chaotic superposition of very sort-path multiples arising from fine layering with nearly random layer properties. Even with perfectly elastic layers having no intrinsic attenuation, stratigraphic attenuation is still present in the analysis of any finite record length. (The word “finite” is important here because the apparent energy loss from stratigraphic attenuation is really just an energy delay and, given an infinite record length, there would be energy conservation.) Both theory and experiment agree that these two attenuation mechanisms are very similar in their effects and nearly impossible to distinguish (Margrave, 2014) such that any practical measure of attenuation will always estimate the combined effect.

Commonly, attenuation measurement has been taken to be equivalent to measuring Q , called the “quality factor” of an anelastic material. Kjartansson (1979) provides a consistent theoretical description of scalar-wave propagation in a “constant Q medium” where the latter refers to a Q value that is independent of frequency but can vary arbitrarily with space. Others (e.g. Aki and Richards (2000)) provide a similar description and there

is general agreement that the amplitude spectrum of a propagating seismic wave decays according to the attenuation law

$$|\widehat{w}_t(f)| = |\widehat{w}_0(f)|e^{-\pi ft/Q} \quad (1)$$

where $|\widehat{w}_0(f)|$ is the amplitude spectrum as emitted by the source (f is frequency), t is traveltime, Q is the aforementioned quality factor, and $|\widehat{w}_t(f)|$ is the wave's amplitude spectrum after propagating for time t . There are a variety of methods of measurement of Q that are discussed in various places such as Cheng (2013) and Tonn (1991). All known methods suffer some degree of instability on real (i.e. noisy) data due largely to the fact that Q appears in the denominator of the exponent of equation 1. Attenuation becomes small when t/Q is small which can happen when t is small, or when Q is large, or some combination of both. The ratio t/Q has been called cumulative attenuation (Hauge, 1981) and here denoted CA . Thus, whenever CA is small, there will be little difference between the initial and attenuated spectra. Suppose the spectrum is measured at two different times t_1 and t_2 with $t_2 > t_1$, then it follows from equation 1 that

$$|\widehat{w}_2(f)| = |\widehat{w}_1(f)|e^{-\frac{\pi f(t_2-t_1)}{Q_{1,2}}} \quad (2)$$

where $|\widehat{w}_1(f)|$ and $|\widehat{w}_2(f)|$ are the amplitude spectra at times t_1 and t_2 , and where $Q_{1,2}$ refers to the interval Q between the position of the wave at time t_1 and its position at time t_2 . For example, suppose we have receivers in a vertical borehole and a source positioned at $z = 0$ next to the borehole (Figure 1). Then a receiver at depth z_1 records $w_1(t)$, enabling the estimation of $|\widehat{w}_1(f)|$, while a receiver at a deeper depth z_2 records $w_2(t)$, and $Q_{1,2}$, called an interval Q , is a property of the interval $z_1 \rightarrow z_2$. A quantity fundamental to attenuation measurements is the "log-spectral ratio" defined as $lsr_{1,2}(f) = \ln[|\widehat{w}_2(f)|/|\widehat{w}_1(f)|]$. It follows from equation 2 that

$$lsr_{1,2}(f) = \ln[|\widehat{w}_2(f)|/|\widehat{w}_1(f)|] = -\pi f(t_2 - t_1)/Q_{1,2} \quad (3)$$

or, upon re-arranging,

$$Q_{1,2} = -\pi f(t_2 - t_1)/lsr_{1,2}(f). \quad (4)$$

Equation 4 shows why Q measurement is unstable because whenever the attenuation is small then lsr is very small (because $|\widehat{w}_2(f)| \sim |\widehat{w}_1(f)|$ and $\ln 1 = 0$) resulting in a very large Q . On noiseless synthetic data, this is not such a problem and a large Q is usually the correct result. However, with real data the presence of noise and other uncontrolled effects means that lsr can often be both small and wildly inaccurate resulting in large Q (even negative Q can happen) with very large errors.

Hauge (1981) proposed estimation of CA instead of Q because it is more stable and because it is really CA that we need to know if the goal is to correct for the effects of attenuation. In the same setting as before, CA is given by

$$CA = (t_2 - t_1)/Q_{1,2} = -lsr_{1,2}(f)/\pi f \quad (5)$$

where we should note that $lsr_{1,2}(f)$ should usually be a negative number because it has been defined using the weaker spectrum (at time t_2) divided by the stronger spectrum (time

t_1). Equation 5 now has the lsr in the numerator and so CA goes smoothly to zero whenever lsr is small.

Transition paragraph

THE SPECTRAL RATIO METHOD OF Q OR CA ESTIMATION

Consider again the experiment depicted in Figure 1 where a seismic source is positioned at the earth's surface near a vertical borehole. The source emits a waveform, $w_0(t)$, which is recorded at level 1 in the borehole and also at the deeper level 2. Using constant Q theory and neglecting wavefront spreading, the first arrival at level 1 can be modelled in the frequency domain as

$$|\hat{w}_1(f)| = |\hat{w}_0(f)|T_1e^{-\pi ft_1/Q}. \quad (6)$$

Compared to equation 1, we now include T_1 representing transmission effects between the source and level 1, and Q_1 is the average Q value between the source and level 1. In a similar fashion, the first arrival waveform at level 2 can be represented as

$$|\hat{w}_2(f)| = |\hat{w}_0(f)|T_2e^{-\pi ft_2/Q}. \quad (7)$$

Now divide equation 7 by equation 6 and take the natural logarithm to find

$$lsr_{1,2}(f) = \ln \frac{|\hat{w}_2(f)|}{|\hat{w}_1(f)|} = \ln \left(\frac{T_2}{T_1} \right) - \pi f \left(\frac{t_2}{Q_2} - \frac{t_1}{Q_1} \right). \quad (8)$$

Defining $T = T_2/T_1$, $\Delta t = t_2 - t_1$, and $Q_{int}^{-1} = \Delta t^{-1}(t_2/Q_2 - t_1/Q_1)$, equation 8 becomes

$$lsr(f) = \ln T - \pi f \frac{\Delta t}{Q_{int}} = \ln T - \pi f CA_{int}. \quad (9)$$

where $CA_{int} = \Delta t/Q_{int}$. Equation 9 predicts that a least-squares fit of a straight line to the measured lsr will have a slope of $m = -\pi f \Delta t/Q_{int}$ and an intercept of $b = \ln T$. Since we expect $T_2 < T_1$, both slope and intercept normally should be negative values.

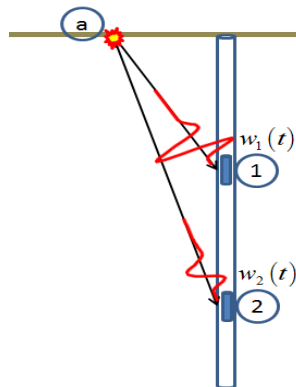


Figure 1: A Seismic source at (a) emits a wave that is recorded in a borehole at level 1 and a deeper level 2. The waveform recorded at level 1 is $w_1(t)$ while at level 2 it is $w_2(t)$.

As described, the spectral-ratio method seems very straight forward but, in practice there are difficulties. Most important is the choice of frequency band over which to do the least-squares fit. In order to see the expected behaviour of equation 9, the amplitude spectra of

both $w_1(t)$ and $w_2(t)$ should significantly exceed noise levels over the range of the fit. A frequency range satisfying this criterion can be difficult to determine, especially for real data with high and variable noise. Even with synthetic data, the useful frequency range is limited by finite-precision computing which has a limited ability to model the strong exponential behaviour of attenuation. Figure 2 shows a typical spectral-ratio calculation for synthetic data that conforms to this theory. Notice that the least-squares fit over 10-60 Hz give a very different linear estimate than a fit over 1-80 Hz. In this case, the 10-60 Hz estimate gives the correct result.

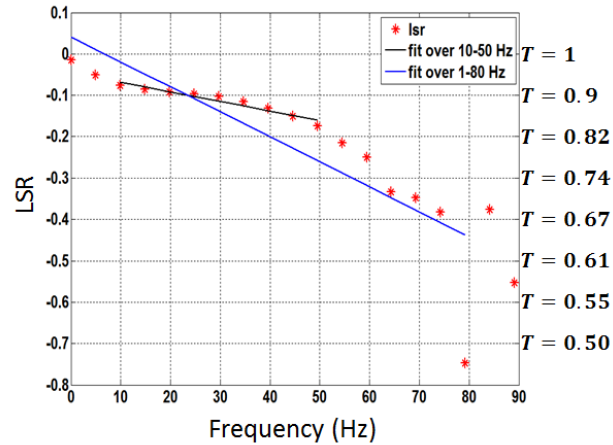


Figure 2: An illustration of a typical spectral-ratio calculation as realized on synthetic data. A least-squares fit over the 10-50 Hz range gives an approximately correct estimate for both Q and T which expanding the frequency range to 1-80 Hz leads to incorrect results as indicated by T greater than 1.0 .

An alternative estimation method that avoids the spectral division needed to form the lsr is the dominant-frequency method. This is a simple variant of the technique introduced by Quan and Harris (1997) who called it the *frequency-shift method*. In this method, the spectra at levels 1 and 2 are measured and then, given a trial Q value called Q_k , an estimate of the level 2 spectrum is constructed from that measured at level 1 by

$$|\hat{w}_{2,k}(f)| = T|\hat{w}_1(f)|e^{-\pi f(t_2-t_1)/Q_k}. \quad (10)$$

This just says that we model the spectrum at level 2 by taking the spectrum at level 1 times a forward Q operator (the transmission coefficient T in this expression will be seen to be irrelevant). Define the dominant frequency for spectrum $|\hat{w}_2(f)|$ as

$$f_{d2} = \frac{\sum_f |\hat{w}_2(f)|^2 f}{\sum_f |\hat{w}_2(f)|^2} \quad (11)$$

with $f_{d2,k}$ being defined by a similar equation. The use of the power spectrum (e.g. $|\hat{w}_2(f)|^2$) in equation 11 is one departure from the method of Quan and Harris (1997) who use the amplitude spectrum and called their frequency the *centroid frequency*. Testing with noisy synthetics indicates that the amplitude spectrum gives too much weight to noisy higher frequencies and that the power spectrum gives better estimates for the dominant frequency.

So, an estimate of the appropriate Q value follows if we can find Q_k such that $f_{d2,k} \cong f_{d2}$. In contrast Quan and Harris (1997) measure both f_{d1} and f_{d2} and develop an analytic formulae relating the frequency shift ($f_{d2} - f_{d1}$) to attenuation but assume the spectrum has a Gaussian shape. In the present method, a scan over the range of reasonable Q values (confined to integer values), computing $f_{d2,k}$ for each is a fast direct search that yields good results and makes no assumptions about spectral shape. Note also that the transmission coefficient T is of no consequence since it cancels out in computing $f_{d2,k}$ by the analog to equation 11. To accomplish this, assume meaningful Q values are expected to fall in the range $Q_{min} < Q < Q_{max}$ where $Q_{min} = 5$ and $Q_{max} = 300$ are convenient bounds, and define

$$Q_k \in [Q_{min}, Q_{min} + 1, Q_{min} + 2, \dots, Q_{max}], \quad (12)$$

so that Q_k is one of the integer Q values falling between Q_{min} and Q_{max} . Next define the objective function

$$O_{f,k} = Q_k (f_{d2} - f_{d2,k})^2 \quad (13)$$

where the use of Q_k on the right-hand-side causes a more pronounced minimum. Experience has shown that better results follow if we modify the objective function to include a second term that matches the width of the spectra $|\hat{w}_2(f)|$ and $|\hat{w}_{2,k}(f)|$, where we define spectral width by

$$\sigma_{d2} = \frac{\sum_f |\hat{w}_2(f)|^2 (f - f_{d2})^2}{\sum_f |\hat{w}_2(f)|^2} \quad (14)$$

and similarly for $\sigma_{d2,k}$. Then the second term will be

$$O_{\sigma,k} = Q_k (\sigma_{d2} - \sigma_{d2,k})^2 \quad (15)$$

and the final objective function is

$$O_k = \frac{O_{f,k}}{\max(O_{f,k})} + \frac{O_{\sigma,k}}{\max(O_{\sigma,k})}. \quad (16)$$

So the estimated Q value will be that Q_k for which equation 16 is minimum.

The dominant-frequency method (DFM) offers a robust alternative to the spectral-ratio method (SRM) and is related to but significantly different from the frequency-shift method (FSM) (Quan and Harris, 1997). Compared to the SRM, the DFM is insensitive to amplitude imbalances because these cancel out in the calculation of dominant frequency and spectral width. The DFM is also much less sensitive to the choice of frequency band although it is not completely insensitive. Compared to the FSM, both methods use a dominant-frequency calculation but the former uses the amplitude spectrum while the latter uses the power spectrum. Also, the DFM makes no assumptions about the spectral shape (the FSM does) and finds the Q estimate by direct search over possible integer values.

DATA ANALYSIS

This work was done on a VSP recorded in the southern United States. This was a zero-offset VSP using a vibroseis source with an 8-96Hz linear sweep. The receivers were three component geophones spaced at 50 ft and extending from 2185ft to 13803ft. Processing of the VSP was done by a third party and a 300ms ribbon of the separated, flattened, downgoing wave is shown in Figure 2a) while Figure 2b) shows the same data after a depth averaging process using an averaging window of ± 400 ft. Essentially each trace of 2b) is the average of all the traces in an 800ft window centered on the corresponding trace of panel 2a). The slight differences are due to residual upgoing waves that have survived the wavefield separation process. As will be seen, much better attenuation estimates arise from the data of 2b) than from 2a).

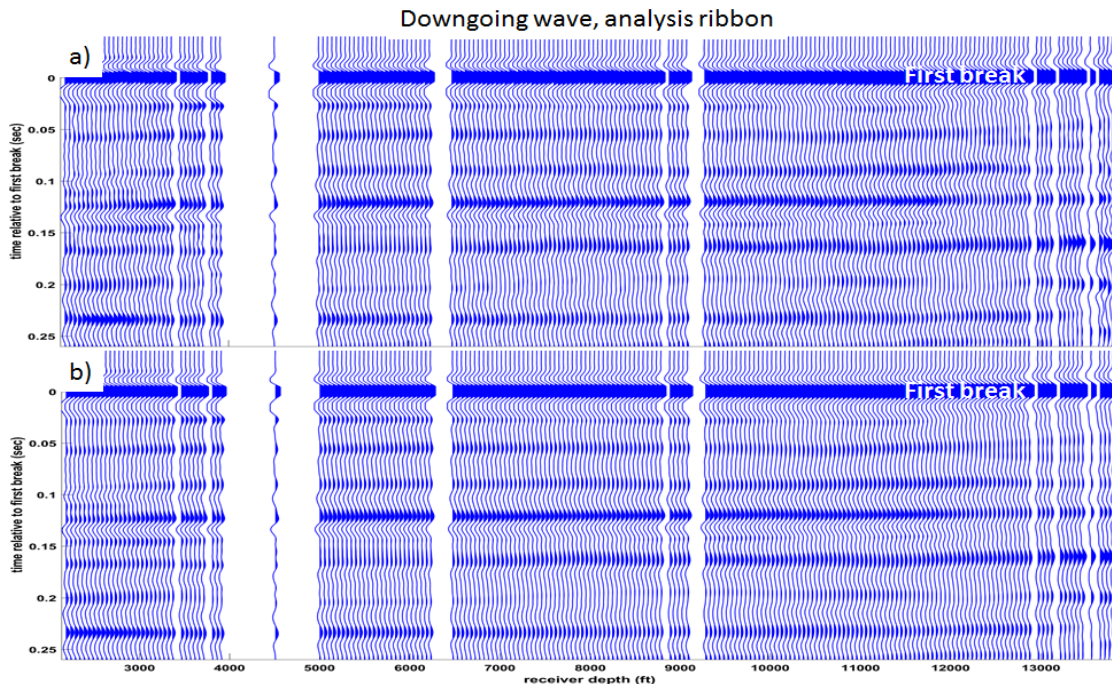


Figure 2: a) A ribbon of data taken from Figure 2 from a window approximately 0.3 sec wide and beginning just before the first breaks. b) The result of spatial averaging of the ribbon in panel a) using an averaging half-width of 400ft. Each trace of panel b) is an average of the traces of panel a) over the depth range ± 400 ft relative to the trace position.

Figure 3 shows the amplitude spectra of the traces in Figure 2. These are the data that will directly determine the attenuation estimates. Both panels of this figure show clear evidence of attenuation as the high frequencies are clearly decaying with depth. The shallowest receiver is at a depth of 2185ft and shows a bandwidth of roughly 10-80Hz while the deepest receiver, at a depth of 13803ft, shows a bandwidth of about 10-55Hz. Despite the high similarity between these panels, the data of Figure 3b) will be shown to give much better attenuation estimates than those of 3a).

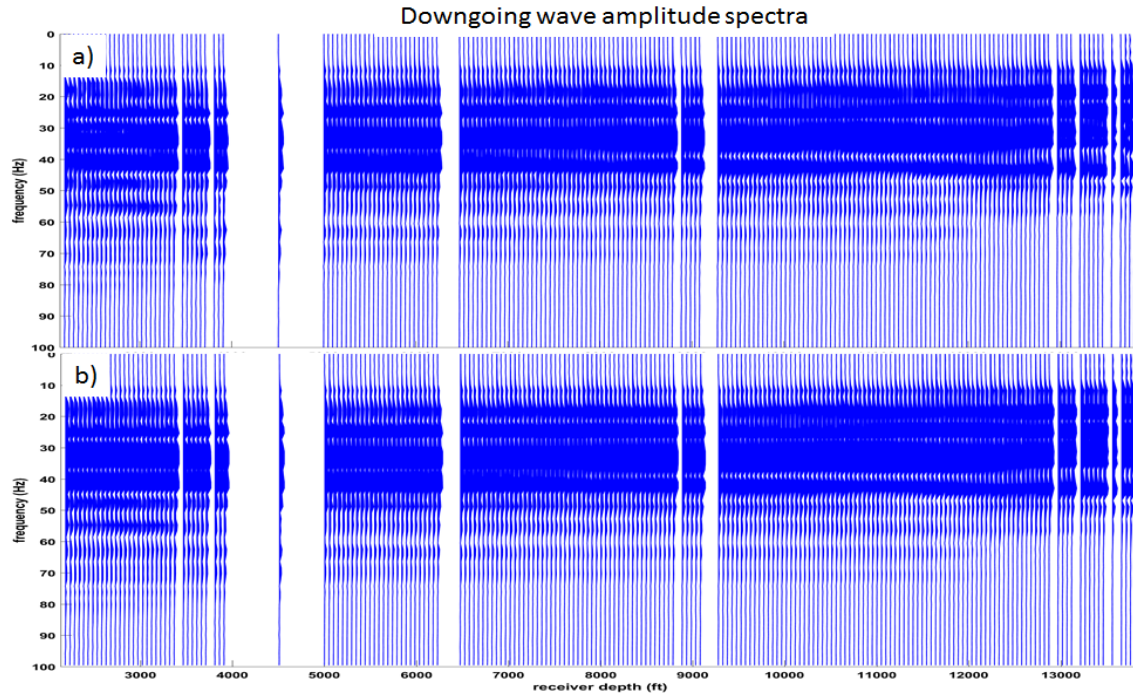


Figure 3: The amplitude spectra of the traces in Figure 2 are shown. The decay of high frequencies with increasing depth is evident in both panels.

Figure 4 is designed to illustrate the SRM (spectral-ratio method) while Figure 5 does a similar thing for the DFM (dominant-frequency method). The figures depict the estimation of Q for three different trace pairs (the same pairs are in both figures). In each case, the reference trace, w_1 , is the data from Figure 2a) at the shallowest receiver. For the shallow case (left column of Figures 4 and 5), w_2 , was chosen to be a receiver at 5000ft, while for the intermediate case w_2 was at 9474ft and for the deep case w_2 was at 13803ft. These traces are shown in the first row of graphs on each figure. The amplitude spectra $|\hat{w}_1|$ and $|\hat{w}_2|$ are in the second row, additionally, Figure 5 gives the measured values of dominant frequency f_{d1} and f_{d2} for both spectra. The computation of these frequencies used equation 11 where the summation range was restricted to the band 8-90Hz. f_{d1} is the same in each case because the reference trace is fixed, but f_{d2} shows clear, progressive decay. The bottom row of both plots shows the actual Q estimate being made. In Figure 4, the lsr is shown in blue together with the least-squares fit of a straight line to a selected frequency range (8-90 Hz) and the estimated Q value. It is clear from these plots that the lsr only shows the expected linear decrease over a limited frequency range. Also clear is the chaotic nature of the lsr which, even in the selected range, is rapidly fluctuating. These fluctuations are caused by spectral notches due to the reflectivity and short-path multiples. The corresponding row in Figure 5 shows the objective function for FDM and the estimated Q value. There is a reasonable correspondence between these two estimates and, given the very different algorithms, this increases confidence in the results.

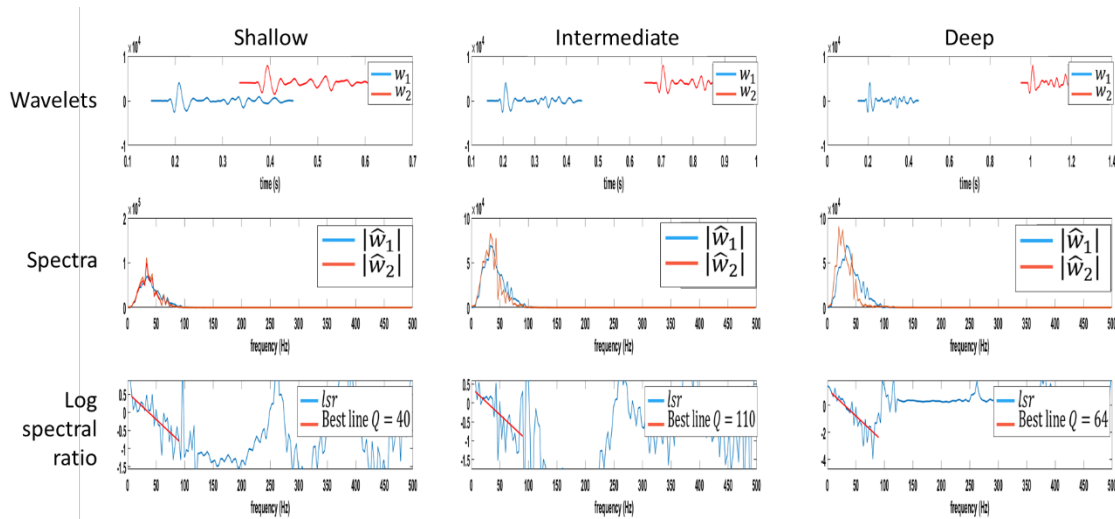


Figure 4: Examples of the spectral-ratio calculation for three different depths: shallow, intermediate, and deep. In each case the reference trace, w_1 , is the same while the comparison trace, w_2 , is moved progressively deeper. These traces are shown in the top panel labelled “wavelets”. In the middle panel are the spectra of the traces and in the bottom panel are the resulting lsr (log-spectral ratio) plots with a red line showing the fitted range (8-90Hz in this case).

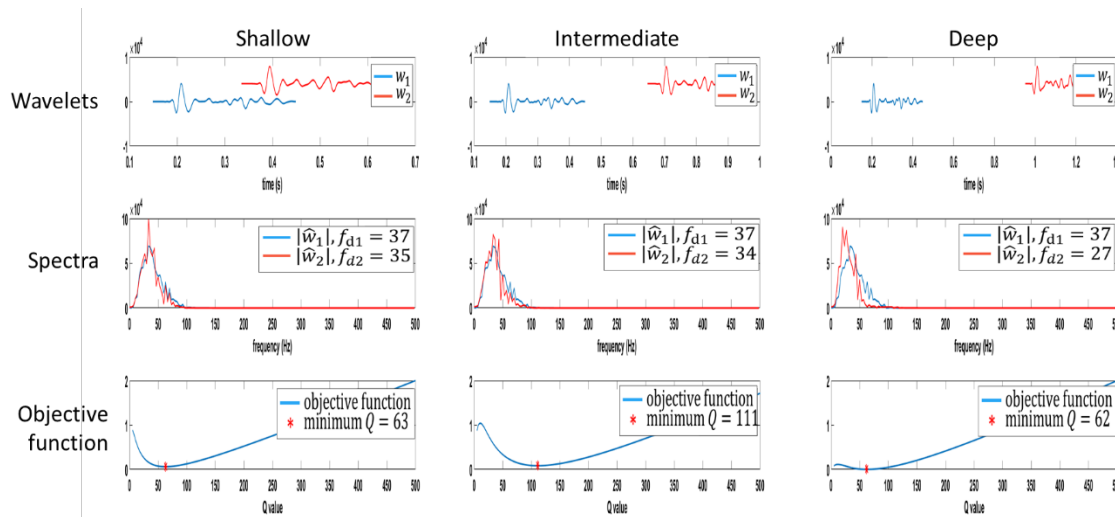


Figure 5: Similar to Figure 4 except that the dominant-frequency method is illustrated. The top panel is identical to Figure 4 and the curves in the middle panel are the same. Also shown in the middle panel are the results of the dominant frequency calculations. In the bottom panel, the objective function is shown together with the estimated Q value. For example, in the intermediate panel, the dominant frequency has decreased from 37 to 34 Hz and a forward Q operator with $Q = 111$, when applied to $|\hat{w}_1|$, reduces its dominant frequency from 37 to 34 as observed with $|\hat{w}_2|$.

Turning now to the presentation of complete Q and CA profiles from the VSP data, first it is useful to examine such profiles computed from a realistic synthetic VSP. For this purpose, well logs (from a different area) were used to synthesize a zero-offset VSP that included very detailed reflectivity, all possible multiples, and a detailed Q model. The Q and CA results are shown in Figure 6. Also of note, the synthetic VSP was computed with exactly separated upgoing and downgoing fields. The Q estimates are all average values references to the most shallow receiver (at 65m) and the CA estimates were computed from

the Q estimates using the first break times (see equation 5). The SRM has great difficulty for the receivers above about 130m because the attenuation is small and it is difficult to get a meaningful lsr and subsequent least-squares fit. In contrast the DFM is much more stable in this interval and gives more realistic estimates. For the deeper receivers, the estimates settle down and become much more similar. Despite these difficulties, the corresponding CA estimates are similar and stable at all depths.

The reason for the relative accuracies of Q and CA via the SRM can be seen by a simple error analysis. For simplicity, assume that least-squares fit to the lsr has resulted in a zero intercept and a slope with value s . Then, from equation 9 we have

$$Q = a\Delta t/s \quad (16)$$

and

$$CA = s/a, \quad (17)$$

where $a = -\pi f$ and the “int” subscript has been dropped. Now suppose that s is in error by δs which is much smaller than s . Then standard error analysis predicts the corresponding errors in Q and CA to be

$$\delta Q = -a\Delta t\delta s/s^2 \quad (18)$$

and

$$CA = \delta s/a. \quad (19)$$

So the error in Q is proportional to the error in s divided by s^2 whereas the error in CA is just directly proportional. When attenuation is low then $|s|$ is very small and division by s^2 is a huge amplification of error. A similar analysis for DFM is not attempted here but empirical observation suggests that it does not have this problem.

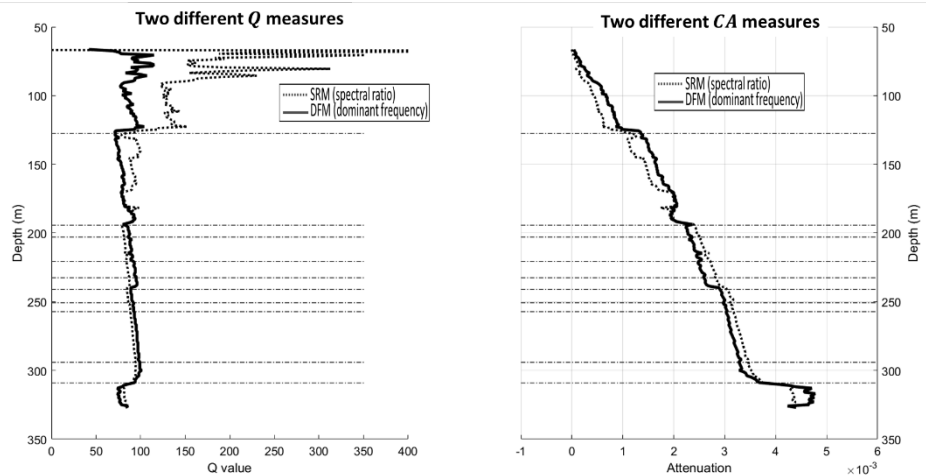


Figure 6: An example of computing Q (left) and CA (right) on a realistic synthetic VSP which included the effects of all multiples, detailed (well log) reflectivity, and a detailed Q model. The geometry of computation was similar to that used on the real data in this paper. The first receiver (at $z=65\text{m}$) was compared to each deeper receiver to deduce an average Q for each depth. The corresponding CA measures were then computed using the first break times and the measured Q .

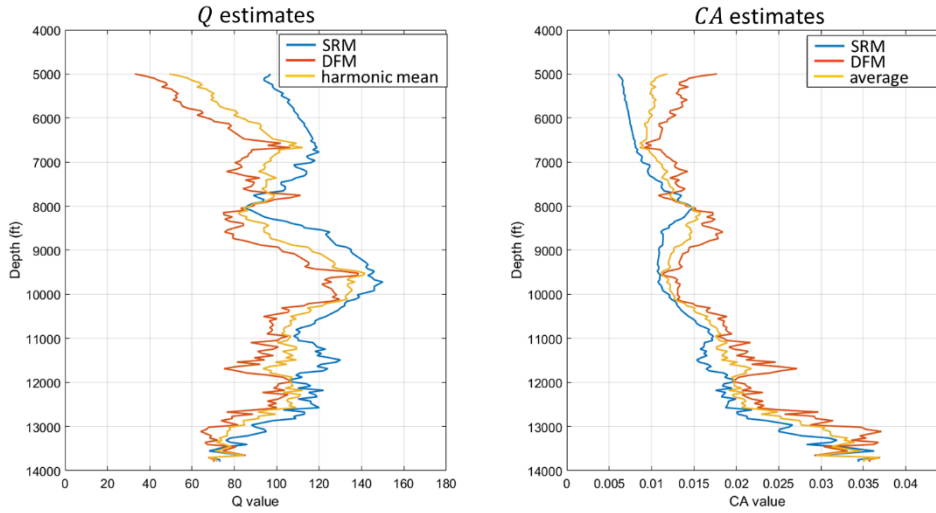


Figure 7: Q and CA estimated from the data of Figure 2a by both the SRM and the DFM. The harmonic mean refers to $Q_{hm}^{-1} = Q_{SRM}^{-1} + Q_{DFM}^{-1}$.

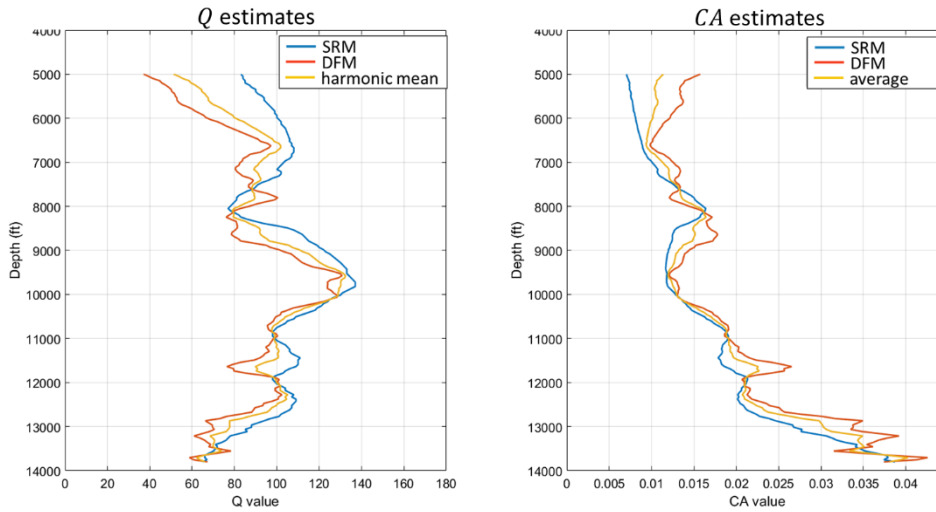


Figure 8: Similar to Figure 7 except that the data were run through a depth averaging process before measurements were made. Each trace was replaced by the average of all adjacent traces within ± 100 ft.

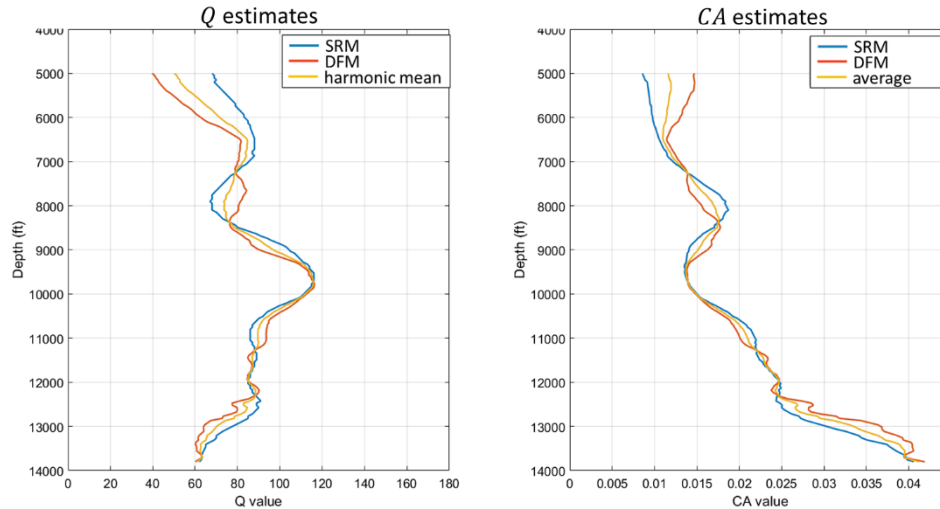


Figure 9: Similar to Figure 7 except that the data were run through a depth averaging process before measurements were made. Each trace was replaced by the average of all adjacent traces within ± 400 ft. The data resulting from this averaging are shown in Figure 2b.

Figure 7 shows the results of Q and CA for the data of Figure 2a. The shallowest receiver (2185ft) was taken as the reference w_1 and the w_2 traces were selected starting at 5000ft and continuing to the deepest receiver. The Q estimates are therefore all average values representing the average effect from 2185ft to the depth noted on the vertical axis. The results from both SRM and DFM track one another quite well but show a lot of fluctuation and the SRM estimates are mostly higher than those from DFM. Shown between the two estimates is the harmonic average (e.g. $Q_{hm}^{-1} = Q_{SRM}^{-1} + Q_{DFM}^{-1}$) which may be a reasonable compromise¹. The CA estimates of Figure 7 were computed from the estimated Q values and the first break traveltimes, while the intermediate curve is the arithmetic average of the two estimates. The rapid fluctuations in these estimates are mostly caused by residual upgoing waves that have survived the wavefield separation process. These can be suppressed by lateral averaging of the data of Figure 2a before the estimation process. Figure 8 shows the results after a very slight averaging where each trace was replaced by the average of those within ± 100 ft. Given the nominal receiver spacing of 50ft, this is roughly a 5:1 averaging. The dramatic reduction of the oscillations is evidence that this is a positive step. Figure 9 shows the results with a larger averaging window of ± 400 ft and the curves are both smoother and the two estimates are in better agreement. This is clearly a judgement call since the true values are unknown but the preference is for consistency between the two methods and smoothness of the result. Larger averaging windows were investigated but the result shown in Figure 9 was preferred.

While the estimates of Figure 9 seem self-consistent and reasonable, they are all referenced to the shallowest receiver at 2185ft and hence are not quite what is needed for seismic data processing. For this purpose, estimated relative to $z=0$ are desired however shallow receivers are generally unreliable, and usually not even attempted, in conventional

¹ The harmonic average was chosen simply because this is the wave that interval Q values “add” to give and average Q .

VSP recording. However, while there was no receiver at the earth's surface, the source was a vibrator with precisely controlled hydraulics designed to radiate a known spectrum. So, it seems that we do know something about the downgoing wave at the earth's surface and a simple assumption is that it is the Klauder wavelet, or autocorrelation, of the sweep. Of course this ignores the spectral modifications due to the vibrator-earth interaction. Baseplate accelerometer recordings or ground-force estimates would be useful to investigate that approach but were not available in this case. A final consideration is that, in theory, a source that emits a wavelet $w_0(t)$ when placed within a homogeneous medium will emit $w_0'(t)$ (the time derivative of $w_0(t)$) when placed on a free surface. This can be understood as the limiting case of a surface ghost from a buried source in the limit as the depth of burial goes to zero. Figure 10 compares the Klauder wavelet for the 8-96Hz linear sweep used in this experiment to its time derivative. In using either of these wavelets as the reference trace, the upper 2185ft of the subsurface will be assigned the attenuation necessary to convert the wavelet's spectrum into the spectrum of the first trace in Figure 3b. So an overall lowering of the Q estimates is to be expected and the estimates should be lower for the time-derivative wavelet than for the Klauder wavelet.

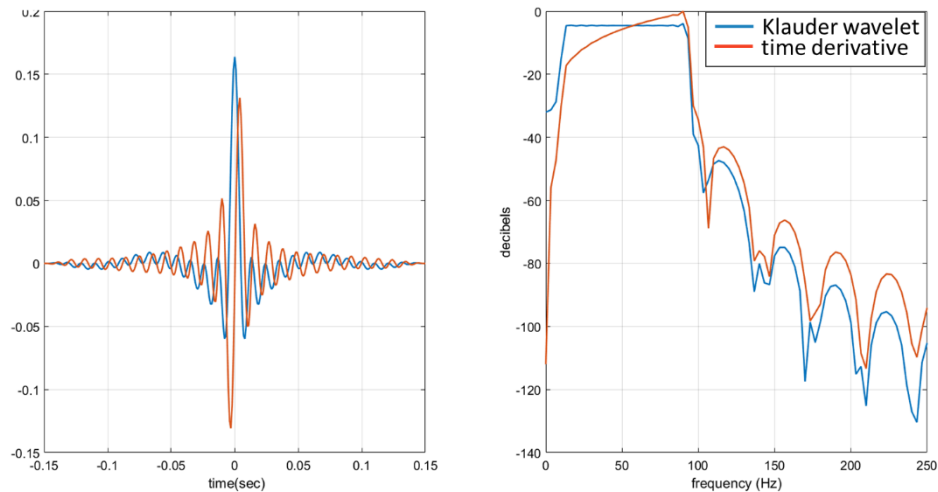


Figure 10: The Klauder wavelet for an 8-96Hz linear sweep (10 seconds long with 0.5 sec taper) is compared with its time derivative in the time domain (left) and the frequency domain (right). The wavelets have been balanced on overall amplitude. The Klauder wavelet has a flat amplitude spectrum over the swept band while the time derivative has more power in the higher frequencies.

Figure 11 shows the resulting attenuation analysis when the reference trace, w_1 , is taken to be the Klauder wavelet at $z = 0$. Not only are the Q values now lower, but the range of estimation has been extended upwards from 500ft to 2185ft. These values are now referenced to $z = 0$ and, in theory, could be suitable input for an inverse Q filter to be applied to surface seismic data. The maximum Q has decreased from about 115 to about 55. It may well be that these values are too low because there are many potential mechanisms that could cause the actual radiated spectrum to lose strength at high frequencies. Figure 12 shows a similar calculation where now the reference trace is the time-derivative Klauder wavelet. The result is Q estimates that are lower still and seem unacceptably so.

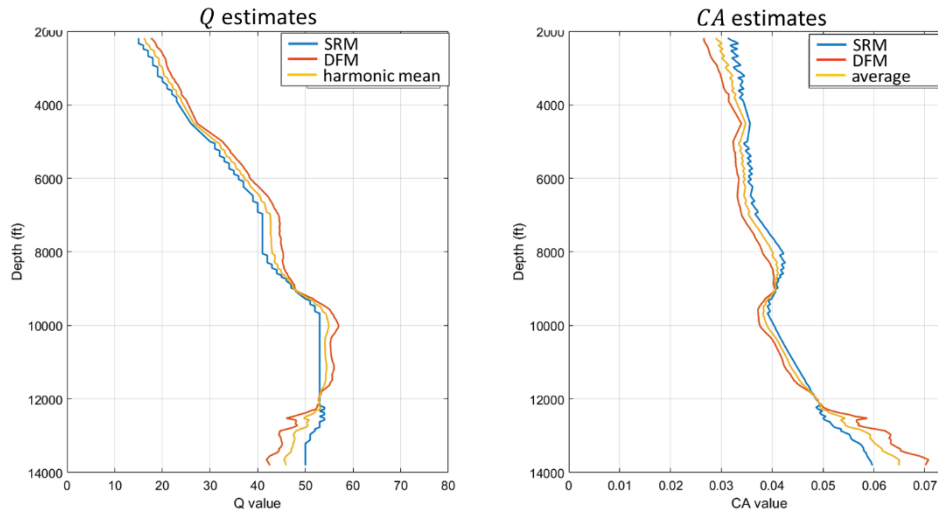


Figure 11: The result of an attenuation analysis where the reference signal, w_1 , is taken to be the Klauder wavelet of Figure 10 at depth $z = 0$. The input data were those of Figure 2b so this result should be compared to Figure 9. Note the change in the depth axis which now extends to 2185ft. The stair-stepping on the Q curve from the DFM happens because that method estimates Q to the nearest integer only. The resulting CA estimate shows saw teeth.

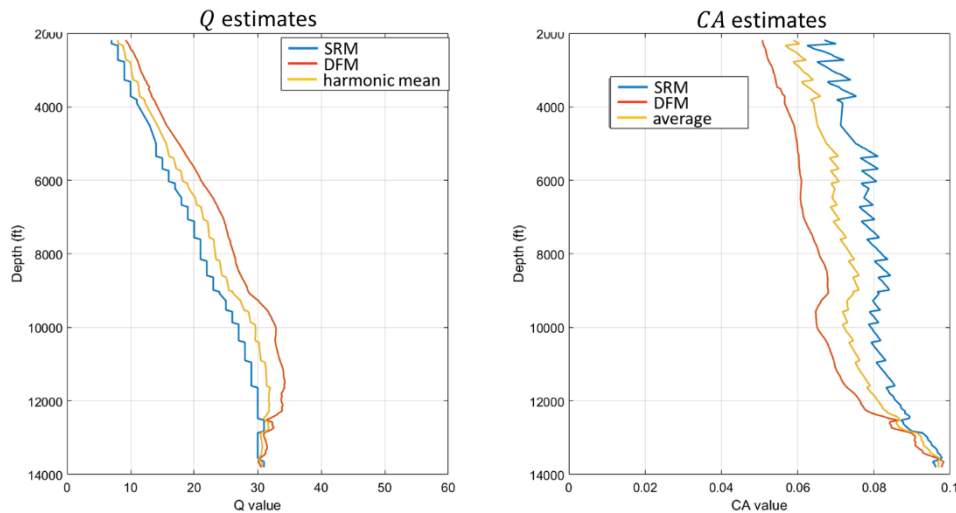


Figure 12: Similar to Figure 11 except that now the reference trace, $w_1(t)$, is taken to be the time-derivative Klauder wavelet (Figure 10). Compare to Figures 11 and 9.

SUMMARY AND CONCLUSIONS

The theory and application of seismic attenuation analysis have been discussed as manifest in the estimation of both Q and CA (cumulative attenuation). Two computational methods were described: the spectral-ratio method (SRM) and the dominant-frequency method (DFM). The SRM is well established and frequency used while the DFM is introduced here. The SRM requires the computation of the log-spectral ratio, lsr , which is the logarithm of the ratio of the amplitude spectra of two wavelets with different propagation times. Theory predicts that the lsr should be a linear function of frequency;

however, this behaviour is only found over a very limited frequency range. Properly specifying this frequency range is the critical decision for a successful result. Q is estimated from the slope of a best-fit line to the linear trend. In contrast, the DFM avoids the spectral division by applying a suite of different forward Q filters to the spectrum of the wavelet with smaller traveltime and Q is predicted by finding the filtered result that best matched the wavelet with longer traveltime. Once a Q estimate is obtained, a CA estimate is then found as the differential traveltime divided by Q . It was demonstrated, and explained theoretically, that, when attenuation is low, CA estimates are much more stable and accurate than Q estimates. These techniques were then demonstrated by application to a zero-offset VSP. Data processing was done to isolate the downgoing wave and 300ms data ribbon beginning at the first breaks was used. Using the shallowest receiver at 2185f as a reference, and attenuation estimated was obtained for all receivers at 5000ft and deeper. It was demonstrated that consistent results were obtained from both estimation methods and, it was argued, this lends credibility to the results. It was also demonstrated that even very small residual upgoing waves in the downgoing field cause considerable instability in the estimates. In a final analysis, the possibility of extending the reference depth to the earth's surface by using the Klauder wavelet, or its time derivative, was examined. This extension resulted in lower Q values as expected but the time-derivative wavelet was considered too extreme. In future work, it would be beneficial to repeat this analysis on other wells and to apply the estimated attenuation values to surface seismic data.

ACKNOWLEDGEMENTS

I thank the sponsors of CREWES, especially Devon Energy, for their support. Devon Energy also provided the data and gave permission to present this work. My thanks to my colleagues at Devon for their insight and suggestions.

REFERENCES

- Bath, M., 1974, Spectral analysis in geophysics: Developments in Solid Earth Geophysics, Vol 7, Elsevier Science Publishing Co.
- Cheng, P., 2013, Anelastic attenuation in seismic data: modelling, measurement, and correction: PhD thesis, University of Calgary.
- Hauge, P. S., 1981, Measurements of attenuation from vertical seismic profiles, *Geophysics*, **48**, 1548-1558.
- Kjartansson, E., 1979, Constant Q-wave Propagation and Attenuation, *Journal of Geophysical Research*, **84**, 4737-4748.
- Margrave, G. F., 2014, Stratigraphic filtering and Q estimation, CREWES Research Report, Volume 26.
- O'Doherty, R. F., and N. A. Anstey, 1971, Reflections on Amplitudes, *Geophysical Prospecting*, **19**, pp. 430-458.
- Quan, Y, and J. M. Harris, 1997, Seismic attenuation tomography using frequency shift method, *Geophysics*, **62**, 895-905.
- Tonn, R., 1991, The determination of seismic quality factor from VSP data: A comparison of different computational methods: *Geophys. Prosp.*, **39**, 1-27.